Pharmacological Reports
https://doi.org/10.1007/s43440-019-00019-8

ARTICLE

Metformin accelerates myelin recovery and ameliorates behavioral deficits in the animal model of multiple sclerosis via adjustment of AMPK/Nrf2/mTOR signaling and maintenance of endogenous oligodendrogenesis during brain self-repairing period

Nima Sanadgol[1] · Mahmood Barati[2] · Fariba Houshmand[3] · Shokoufeh Hassani[4] · Tim Clarner[5] · Mohsen shahlaei[6] · Fereshteh Golab[7]

Received: 3 May 2019 / Revised: 25 August 2019 / Accepted: 5 September 2019

Abstract

Background Multiple sclerosis (MS) is a devastating autoimmune disorder characterized by oligodendrocytes (OLGs) loss and demyelination. In this study, we have examined the effects of metformin (MET) on the oligodendrogenesis, redox signaling, apoptosis, and glial responses during a self-repairing period (1-week) in the animal model of MS.

Methods For induction of demyelination, C57BL/6 J mice were fed a 0.2% cuprizone (CPZ) for 5 weeks. Thereafter, CPZ was removed for 1-week and molecular and behavioral changes were monitored in the presence or absence of MET (50 mg/kg body weight/day).

Results MET remarkably increased the localization of precursor OLGs ($NG2^+/O4^+$ cells) and subsequently the renewal of mature OLGs (MOG^+ cells) in the corpus callosum via AMPK/mammalian target of rapamycin (mTOR) pathway. Moreover, we observed a significant elevation in the antioxidant responses, especially in mature OLGs (MOG^+/nuclear factor erythroid 2-related factor 2 ($Nrf2^+$) cells) after MET intervention. MET also reduced brain apoptosis markers and lessened motor dysfunction in the open-field test. While MET was unable to decrease active astrogliosis (GFAP mRNA), it reduced microgliosis by down-regulation of Mac-3 mRNA a marker of pro-inflammatory microglia/macrophages. Molecular modeling studies, likewise, confirmed that MET exerts its effects via direct interaction with AMPK.

Conclusions Altogether, our study reveals that MET effectively induces lesion reduction and elevated molecular processes that support myelin recovery via direct activation of AMPK and indirect regulation of AMPK/Nrf2/mTOR pathway in OLGs. These findings facilitate the development of new therapeutic strategies based on AMPK activation for MS in the near future.

Keywords AMPK · Cuprizone · mTOR · Multiple sclerosis · Nrf2

✉ Fereshteh Golab
fgolab520@gmail.com; golab.f@iums.ac.ir

[1] Department of Biology, Faculty of Sciences, University of Zabol, Zabol, Iran

[2] Department of Biotechnology, Faculty of Allied Medicine, Iran University of Medical Science, Tehran, Iran

[3] Department of Physiology, School of Medicine, Shahrekord University of Medical Sciences, Shahrekord, Iran

[4] Toxicology and Diseases Group, Institute of Pharmaceutical Sciences (TIPS), Tehran University of Medical Sciences, Tehran, Iran

[5] Institute of Neuroanatomy, Faculty of Medicine, RWTH Aachen University, 52074 Aachen, Germany

[6] Nano Drug Delivery Research Center, School of Pharmacy, Kermanshah University of Medical Science, Kermanshah, Iran

[7] Cellular and Molecular Research Center, Iran University of Medical Science, P.O. Box 14155-6451, Tehran, Iran

Published online: 18 December 2019

Introduction

Multiple sclerosis (MS) is a devastating autoimmune demyelinating disease of the central nervous system (CNS). Lesions in the MS are described by chronic neuroinflammation, reactive gliosis and oligodendrocytes (OLGs) loss [1]. T lymphocytes are the key players of the MS pathobiology, and reactive oxygen spices (ROS) have been widely implicated in the adaptive immune response through activation of these cells [2]. Interferon-beta (IFN-β) is the most used first-line intervention in relapsing–remitting forms of multiple sclerosis (RRMS) and able to modify the course of the disease through multifactorial mechanism of action (initially act as an immunomodulatory agent in MS) [3]. Recently, activation of AMP-activated protein kinase (AMPK) was shown to induce signaling downstream of stimulator of interferon genes (STING) and promote innate immune signaling [4]. Also, it has been shown that AMPK interferes with interferon-gamma (IFN-gamma), which activates astrocytes/microglia and its activity is decreased in the CNS at the onset and exacerbation of experimental autoimmune encephalomyelitis (EAE) [5]. Because mitochondrial dysfunction and excessive ROS observed in MS, and oxidative stress is regulated, in part, by, AMPK we postulated that metformin (MET)-induced AMPK activation could be neuroprotective in our animal model; however, its function has yet to be been defined. Among serine/threonine protein kinases (STPK), AMPK acts as an energy controller in the cell and enrolled in the response to energy imbalance, e.g. glucose starvation or ATP depletion [6]. Activation of AMPK affects other important members of STPK named the mammalian target of rapamycin (mTOR) and consequently reduces the consumption of ATP in addition to increased production of it in the cell [7]. Accordingly, activated AMPK enhances the endothelial function, reduces the inflammatory response, and adjusts redox balance via regulation of mitochondrial metabolism [8]. Another factor that regulates the equilibrium of cellular redox is nuclear factor E2-related factor 2 (Nrf2). Nrf2 is a leucine zipper family transcription factor, having an important role in the defense of cell against oxidative stress [9]. On the other hand, the interaction between AMPK and ROS are complex and it has been demonstrated that AMPK potentially acts as a downstream target of ROS [10]. It was reported that in the endothelial cells, AMPK exerts its anti-apoptotic effects through the elimination of ROS [11]. It was also shown that the activation of AMPK reduced oxidative stress by changing the activity or level of nicotinamide adenine dinucleotide phosphate (NADPH) oxidase, cyclooxygenase-2 (Cox2), inducible nitric oxide synthase (iNOS), or manganese superoxide dismutase (SOD) [12]. The underlying mechanisms and consequences of AMPK activation in neurodegenerative disorders remain mostly uncharacterized. Recently, results from the EAE model have shown that supplementation with an AMPK activator 5-amino-4-imidazole carboxamide riboside (AICAR) may provide greater efficacy against MS [13]. Khan et al. [14] also showed that genetic inactivation of AMPK exacerbates clinical signs in the EAE model. Another study showed that during reactive gliosis, up-regulated AMPK in activated astrocytes playing an important role in the prevention of astrocyte apoptosis [15]. Surprisingly, Ajaib et al. have demonstrated that AMPK has effects on the survival of oligodendrocytes and restore the integrity and function of CNS in EAE model [16]. The most commonly used models for studying de and remyelination is CPZ, a copper chelating agent, and its feeding could induce reversible myelin loss in several brain regions, particularly in the corpus callosum (CC) [17]. During CPZ treatment blood–brain barrier (BBB) is intact and consequently, local injuries happen without interfering of autoimmune responses [18]. As MET is able to crossing the BBB, for the first time, we have explored the effects of MET in the autonomous myelin recovery after CPZ challenge. Our data addresses a series of pathways involved in the protection ensured by MET to favor the viability of OLGs and the preservation of myelin. The pathways addressed herein are intertwined and crosstalk to apoptosis, oxidative status, autophagy and relevant metabolic pathways that may justify the observed effects under MET treatment. In this study, we show the significance of MET as a therapeutic factor in the oligodendrogenesis and related disorders such as MS.

Materials and methods

Induction of toxic demyelination

7–8 weeks (18–20 g) male C57BL/6 mice were bought from Pasteur Institute, Tehran, Iran. Mice were maintained at standard temperature (20–22 °C), 12 h light/dark cycle with free access to water and food. With 5 weeks consumption of 0.2% CPZ mixed into normal rodent chow demyelinating phenotype was induced in mice. Animal handlings were approved by the laboratory animal's ethic committee, in Iran University of Medical Sciences (IUMS) with maximum efforts for reducing of animal's number and their suffering.

Determination of metformin effective dose

To examine which doses of MET is suitable for this study mice were intraperitoneal (*ip*) administered with four doses of MET (25, 50, 100, 200 mg/kg/body weight per

day dissolved in normal saline) during recovery period and average body weight (ABW), and mortality were monitored every day. We found that higher doses of MET (100, 200 mg/kg) considerably decrease ABW of mice and resulting in higher mortality. In comparison, 25 and 50 mg/kg of MET administration did not significantly affect ABW and mortality than the other doses (data not showed). So, effective dose (50 mg/kg/day) selected as an intervention concentration. This optimized concentration of MET was relatively in accordance with previous in vivo studies in different animal models [19, 20]. It should mention that usual MET doses that are given to adult (70 kg body weight) diabetes type 2 patients are between 15 mg/kg/day (orally twice a day) and 37 mg/kg/day (orally in divided doses).

Free and MET recovery periods

Mice randomly divided into four groups ($N=20$ per group): (1) control group; animals fed normal diet (ND) for 6 weeks beside injection (*ip*) of normal saline (250 µl) as vehicle every day in last week, (2) model group; animals fed 0.2% CPZ mixed in ND for 5 weeks, and then passed 1-week recovery without CPZ besides everyday vehicle injection (free recovery period); (3) treatment group; model group that received 50 mg MET throughout 1-week recovery (MET recovery period); (4) MET control group; control group that received 50 mg MET throughout the last 7 days (Fig. 1a).

Behavioral analysis

At the end of experiments, five randomly selected mice of each group were evaluated via the open-field test for motor impairment analysis. The locomotion of animals in the center of the box (50 × 50 cm) was monitored during the standard period (5 min) by an overhead camera. Using tracking system (EthoVision, Noldus Information Technology Co., Wageningen, Netherlands) motor function evaluated through measuring the velocity of movement (cm/s), total moved distance (cm), and duration of moved in the central zone (s). The ratio of traveled distance in the central zone (DC) over the total moved distance (TD) has also been calculated (DC/TD) as a sign of anxiety [21].

Tissues preparation and LFB staining

At the end of behavioral assessments, six randomly selected mice of each group were euthanized using *ip* injection of xylazine (4 mg/kg) and ketamine (50 mg/kg), and

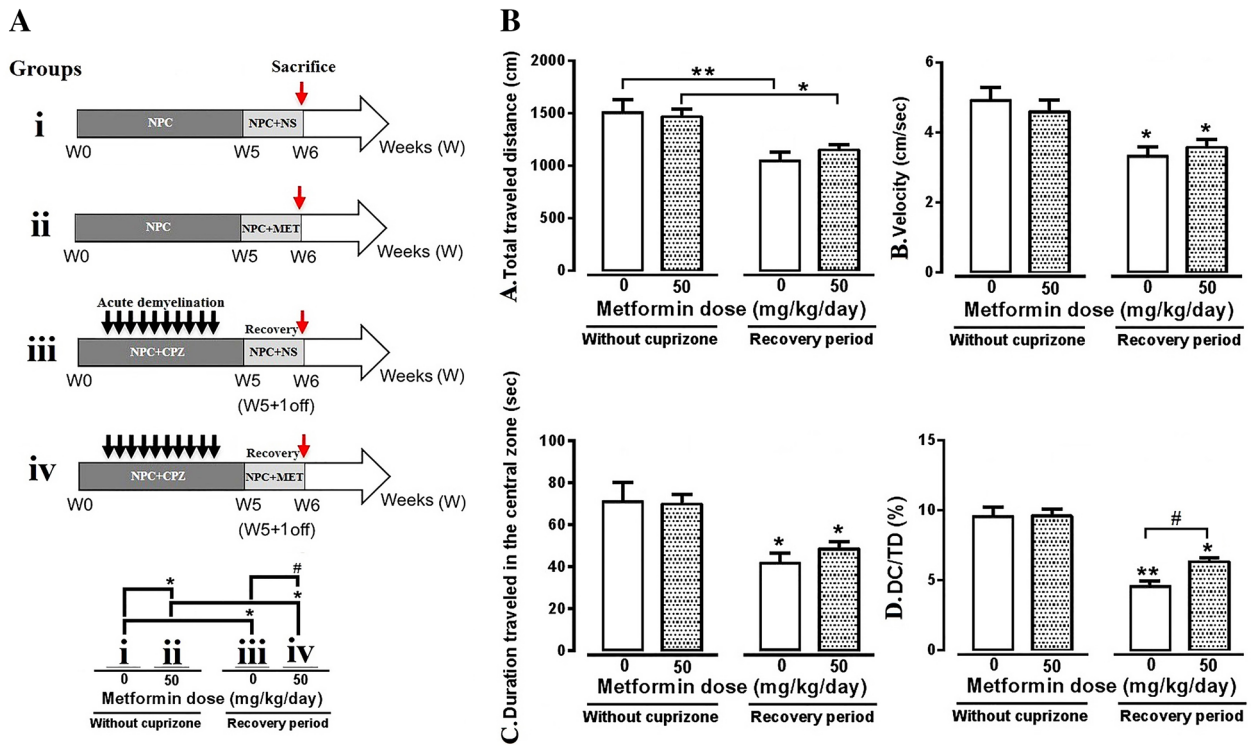

Fig. 1 Experimental design (**a**, up) and symbols of relevant groups comparison (**a**, down). Effects of metformin (MET) on behavior of mice in the open-field test (**b**). Data analysis showed that MET (50 mg/kg, *ip*, $n=5$) significantly decreased ($p<0.05$) anxiety via increasing DC/TD ratio (*D*). Data are presented as means ± SEM, analyzed using tow-way ANOVA. *Compared to relevant control mice, #compared to free recovery, (*,#$p<0.05$; **$p<0.01$) with Bonferroni's correction for multiple comparisons

transcardially perfused with phosphate buffer saline (PBS, pH 7.4) and then with 4% paraformaldehyde dissolved in PBS. Brains removed from the skull and post-fixed in 4% paraformaldehyde (v/v in PBS) at 4 °C overnight. Afterward, brains were rinsed in 30% ice-cold sucrose in PBS. Then tissues fixed in the optimal cutting temperature compound (OCT, Tissue Tek) and kept in − 80 °C. Later, 5 µm thickness coronal section of each fixed brain were provided and distance between 1.58 to 2.30 mm from the bregma was selected using mouse brain atlas. In all histological analyses, the rostral part of the CC was used as the target region. Moreover, phenotypes of myelin fibers were evaluated via staining of some sections with luxol fast blue (LFB) as described previously [22].

Transmission electron microscopy (TEM)

After euthanizing mice were transcardially perfused with 4% PFA and 2% glutaraldehyde dissolved in 0.1 M cacodylate buffer (pH 7.4) respectively. Brains removed from the skull and post-fixed in 1% Osmium tetroxide (OsO_4) in 0.1 M PBS for 60 min. The brain coronal slices consist of CC region were isolated, gently washed in cold 0.1 M PBS, serial dehydrated in ethanol and afterward immersed for 15 min in 100% acetone, and finally embedded in epoxy resin. Coronal sections contained white matter of CC confirmed by toluidine blue staining. The embedded tissues were cut into ultrathin sections (0.1 µm), contrasted with aqueous uranyl acetate and lead citrate and mounted on copper mesh grids (Electron Microscopy Sciences). The ultra-structure of myelin sheaths was observed using a Zeiss EM900 transmission electron microscopy (TEM, magnification, ×20,000; Carl Zeiss AG, Jena, Germany) at 80 kV. In order to analyze the density of myelinated axons, TEM images were imported into ImageJ software. Based on the number of myelinated axons in the 500 μm^2 at ×7000, the density of axons calculated and thickness of myelin sheath in individual axonal fibers measured via calculation of g-ratio (axon diameter/diameter of axon plus the myelin sheath) from at least 50 randomly chosen axons per mouse and three mice per group.

Immunofluorescence (IFS) analysis

IFS analyses were performed as described previously [23, 24]. In brief, the dried sections were rehydrated for 20 min in 0.1 M PBS, incubated in blocking solution, and then incubated for 1 h in permeabilization buffer. Prepared sections incubated with related primary and secondary antibodies dissolved in antibody solution (5% goat serum, 0.05% Triton X-100 in PBS). Used primary monoclonal antibodies were: mouse anti-neuron glial-2 (NG2, 1:500; bio-rad), and rabbit anti-Olig4 (O4, 1:500; bio-rad) as markers of OLGs progenitor cells (OPCs), mouse anti-MOG as marker of mature OLGs (1:500; Millipore), rabbit anti-p-AMPK as marker of active AMPK (1:500; bio-rad), rabbit anti-p-mTOR as marker of autophagy (1:300; Santa Cruz Biotechnology) and rabbit anti-p-Nrf2 as marker of antioxidant respond (1:300; Santa Cruz Biotechnology). The secondary antibodies were FITC conjugated goat anti-mouse IgG for detection of NG2 and MOG and TR conjugated goat anti-rabbit for detection of O4, p-AMPK, p-mTOR and p-Nrf2 (1:1000; Santa Cruz Biotechnology). Moreover, for detection of MOG, we also used HRP conjugated goat anti-chicken IgY (1:1000; Santa Cruz Biotechnology). Counterstaining and visualization of a nucleus for IFS sections were performed via DAPI staining [23, 24].

Monitoring of redox signaling and ADP/ATP ratio

After euthanizing mice were transcardially perfused with cold PBS (50 ml) and three brains in each group were rapidly removed. Rostral CC and nearby regions were dissected in ice and kept at − 80 °C. At the time of experiment, tissue was homogenized and centrifuged (3000 rpm for 10 min) and then supernatants were used for future assessments. Quantity of protein in homogenates was measured by Bicinchoninic Acid (BCA) protein assay method (Sigma-Aldrich). The activity of catalase (CAT), superoxide dismutase (SOD), glutathione peroxidase (GPx), as well as the determination of reactive oxygen species (ROS), lipid peroxidation (TBARS), and total thiol were performed according to standard protocols [25–29]. On the other hand, extracellular ADP/ATP ratio was assessed using ion pair-high performance liquid chromatography (IP-HPLC) in the homogenate of tree brains in each group [30].

Quantitative reverse transcription PCR (qRT-PCR)

Total RNA extraction, cDNA synthesis, and qRT-PCR were performed as described before [31]. In brief, three CC tissues in each group were provided in the same way that described in the previous section and then dissected in DEPS water and placed at − 80 °C. RNA was isolated according to the AccuZol™ (BIONEER) manufacturer's instructions and resolved in 50 µl DEPS water. Then polymerization of cDNA was performed using 5 µg RNA as a template by AccuPower ready-to-use reverse transcription kit (BIONEER). 1 µg of synthesized cDNA used for SYBR Green-based real-time PCR via 2X Greenstar qPCP kit (BIONEER). Amplification conditions were 95 °C for 10 min (one cycle), 95 °C for 20 s (one cycle) and 58 °C for 45 s (one cycle) followed by 95 °C for 30 s (40 cycles). Finally, β-actin standards were used for sample normalization and by $\Delta\Delta C_t$ method relative expression changes were calculated. The sequences of primer were used in this manuscript are shown in Table 1.

Table 1 Sequence of specific primers used for quantitative real-time revers transcription PCR

	Gene name	Primer sequence
GFAP	Forward	5′-AGGTGGAGAGGGACAACTTTG-3′
	Reverse	5′-TTCATCTGCCTCCTGTCTATACG-3′
MOG	Forward	5′-CGTCTCTGGAAGAACAAAGGTC-3′
	Reverse	5′-AGAGTACATCATGCCGACTGC-3′
MAC-3	Forward	5′-GACACACGATGGAAGCAGTTG-3′
	Reverse	5′-AAATTCACAGCCCAAGAGACAG-3′
NG2	Forward	5′-AATGAGGACCTGCTACACGG-3′
	Reverse	5′-CATCTGTAGTCAACAGCCGC-3′
Nrf2	Forward	5′-CATGATGGACTTGGAGTTGCC-3′
	Reverse	5′-TGTCTTGCCTCCAAAGGATGTC-3′
*N*ogo-*A*	Forward	5′-TACTTACGTTGGTGCCTTGTTC-3′
	Reverse	5′-ATGATCTATCTGCGCCTGATGC-3′
O4	Forward	5′-GACAGAGAATGCCTCCCAGA-3′
	Reverse	5′-ATCACTTCCCGCAGACCA-3′
PLP	Forward	5′-AATTCCCAGCTGACGGAGATCACA-3′
	Reverse	5′-TCTACTCGAAGCCTTGTCAGCACA-3′
β-actin	Forward	5′-TGAAGATCAAGATCATTGCTCCTC-3′
	Reverse	5′-TCAGTAACAGTCCGCCTAGAAG-3′

Flow cytometry assessment

Three animals in each group were anesthetized as described above, perfused with 50 ml cold PBS and brains were quickly detached and hemispheres were separated, freed from meninges, placed into ice-cold digestion buffer in PBS (DNase I, 1 mg/ml of collagenase D), and cut into small pieces and then incubated at 37 °C for 30 min. After incubation to stop the enzymatic digestion PBS was added and cells passed through a 70 µm nylon cell strainer (Becton–Dickinson) and centrifuged (2000 rpm, 5 min, 4 °C). After aspiration of supernatant, the pellet re-suspended in 40% and laid on the 70% Percoll solutions (Amersham Pharmacia Biotech). After centrifuging (2000 rpm, 25 min, room temperature) the cells were collected from the interface and transferred to a separate tube, washed twice with HBSS containing 10% fetal bovine serum (GibcoBRL) and fixed in 4% formaldehyde (20 min in ice). Subsequently, cells incubated (45 min, 4 °C) in the mixture of anti-O4 and NG2 primary monoclonal antibodies in flow cytometry buffer (FCB). After washing, cells incubated (45 min, 4 °C) with secondary antibodies. Then, the samples centrifuged (3000 rpm, 10 min) and cells washed twice and re-suspended in FCB. Finally, samples were run on a FACSCalibur Flow Cytometer (BD Biosciences) and evaluated using FlowJo software [32].

Western blotting (WB)

Western blot analysis was done as described before [22, 23]. In brief, three CC tissues in each group were provided in the same way that described in qRT-PCR section and homogenized with complete protease inhibitor cocktail (Roche, Mannheim, Germany), centrifuged and protein concentrations were estimated by BCA protein assay method (Sigma-Aldrich). Proteins (50 µg) were resolved on 12.5% SDS-PAGE gels and via electrophoretic transfer system (Bio-Rad, Munchen, Germany) bonds moved to polyvinylidene fluoride (PVDF) membranes. After blocking of membranes with 5% milk they incubated (4 °C overnight) with primary antibodies (1:500) including rabbit anti-Bax, Bcl-2, cleaved caspase-3 and α-tubulin (Santa Cruz Biotechnology). Next membranes were carefully washed with PBS-T (PBS, 0.05% Tween-20), and incubated (4 °C, 4 h) with horseradish peroxidase (HRP) conjugated goat anti-rabbit secondary antibodies (1:1000, Santa Cruz Biotechnology). The blots were exposed to DAB (3, 3′-diaminobenzidine and H_2O_2) solution for detection of target antigens. Finally, quantification of band intensities was performed by ImageJ software (version 1.49) after background subtraction and normalization of the density of each band to the density of α-tubulin.

In silico analyses

Molecular docking was performed using the AutoDoc4. To this end, first the 3-D structures for AMPK, Keep1, MTORC1, and MTORC2 proteins were first obtained from the RCSB protein database with access codes of 5KQ5, DYH2, 5H64 and 5ZCS respectively. The water molecules in the structures were manually removed and gastiger partial charges were added to atoms by auto-dock tools software. Structural sketching and optimization of MET were done in Avogadro software, and molecular energy minimization conducted using the static algorithm. The partial charges of the atoms were calculated and all rotational bands were considered as active. Energy maps for involved atom types were obtained using the autogrid4 tool, and a 250-run for each docking was performed under the Lamarck's genetic algorithm. Output structure images were prepared in VMD software.

Statistical analysis

The MET effects on each studied parameter were examined using a two-way analysis of variance (ANOVA). For multiple group comparisons, Bonferroni post hoc test was used and the results were considered significant at $p < 0.05$.

Results

Metformin promotes recovery of motor impairment

The general locomotors activity and anxiety were measured via distance moved and velocity, as well as traveled distance in the central zone of the open-field, respectively. As predicted, CPZ challenge considerably induced motor impairment and even after 1-week free recovery period, total traveled distance ($p < 0.01$), movement velocity ($p < 0.05$), duration traveled in the central zone ($p < 0.05$) and percentage of DC/TD ratio ($p < 0.01$) were lower compared to control group (Fig. 1b). Metformin administration during the 1-week recovery period (MET recovery group) notably improved anxiety via increasing DC/TD ratio ($p < 0.05$) compared to the free recovery group (Fig. 1b). It is notable that total traveled distance, movement velocity, duration traveled in the central zone and percentage of DC/TD ratio were still significantly ($p < 0.05$) lower in the MET recovery group compared to the relevant control group (Fig. 1b).

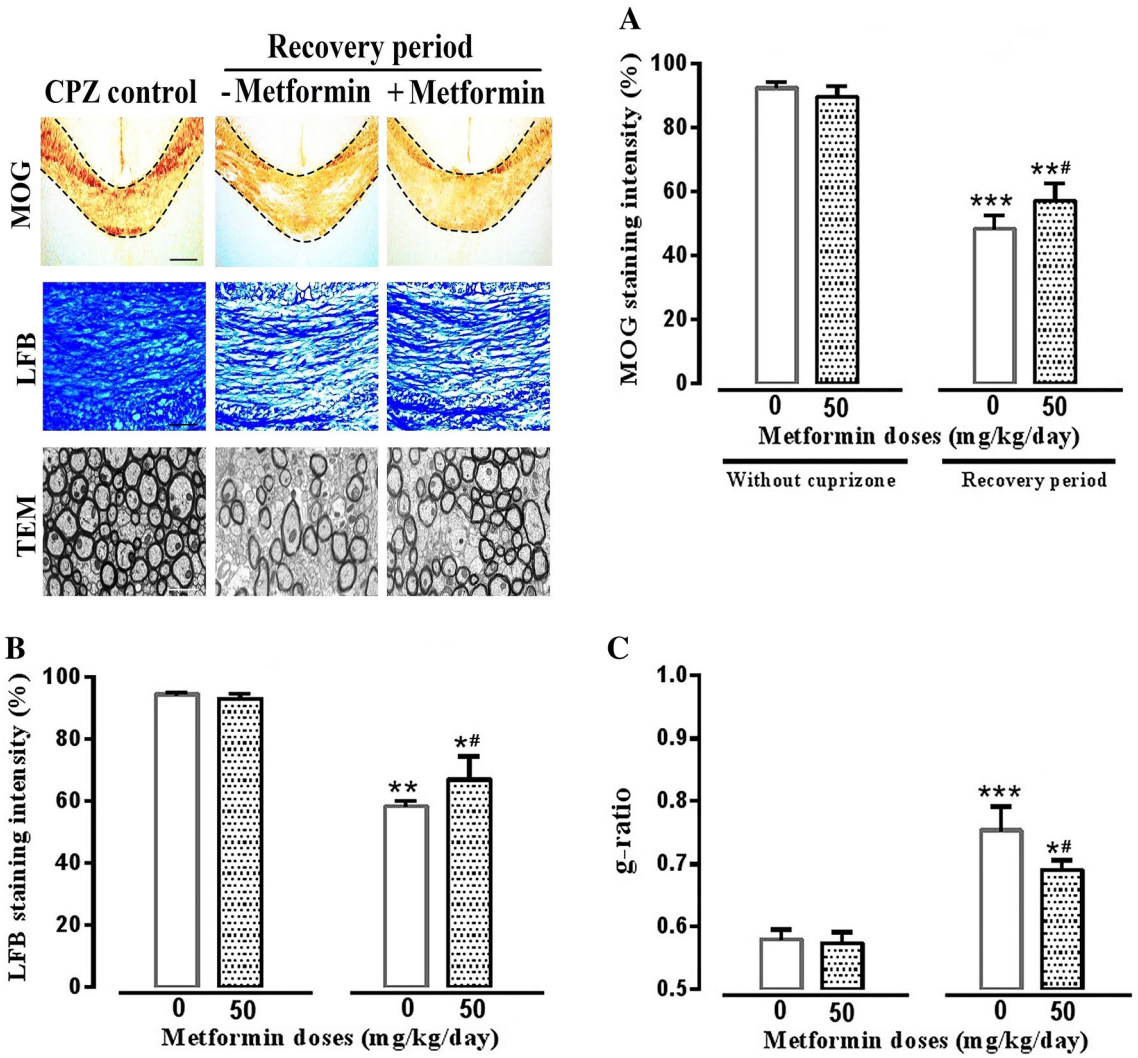

Fig. 2 Evaluation of effects of metformin (MET) in myelin markers by IHC of myelin oligodendrocyte glycoprotein (MOG, up panels), luxol fast blue stain (LFB, middle panels) and transitional electron microscopic (TEM, down panels) in the corpus callosum (CC) (**a**–**c**). Quantification of all myelin markers show that recovery with MET significantly increased remyelination in CC region ($p < 0.05$, **a**, **b**). Metformin recovery group exhibited an accelerating effect on myelin reconstruction and repair indicating as g-ratio ($p < 0.05$) in TEM analysis ($p < 0.05$, **c**). Scale bar = 50 µm. Data are presented as mean ± SEM, analyzed using tow-way ANOVA. *Compared to relevant control mice, #compared to free recovery, ($^{*,\#}p < 0.05$; $^{**}p < 0.01$; $^{***}p < 0.001$) with Bonferroni's correction for multiple comparisons

Metformin increased myelinating oligodendrocytes and decreased microglial activation

Sections from CC region of each brain were stained with both LFB which stains the lipid-rich myelin sheath blue, and anti-myelin oligodendrocyte glycoprotein (MOG) antibody which stains the MOG protein brown (IHC), moreover, TEM analysis provided a subjective assessment of the myelin sheath loss in the rostral CC (Fig. 2a–c). As predicted, even after 1-week of the free recovery period, the myelin level was reduced compared to the control group (Fig. 2a–c). MET recovery group had a significant ($p < 0.05$) positive effect on MOG and LFB density compared to the free recovery group (Fig. 2a, b). MET recovery group exhibited a significant effect on myelin reconstruction and repair indicated in TEM analysis compared to the free recovery group ($p < 0.05$, Fig. 2c). Moreover, using qRT-PCR, the effects of MET on mRNA expression of activated microglial (Mac-3), and astrocytes (GFAP) markers besides myelin proteins (MOG and PLP) were tested on CC region of mice after 1-week recovery (Fig. 3a–d). PCR analysis demonstrated a considerable increase in mRNA expression of both myelin

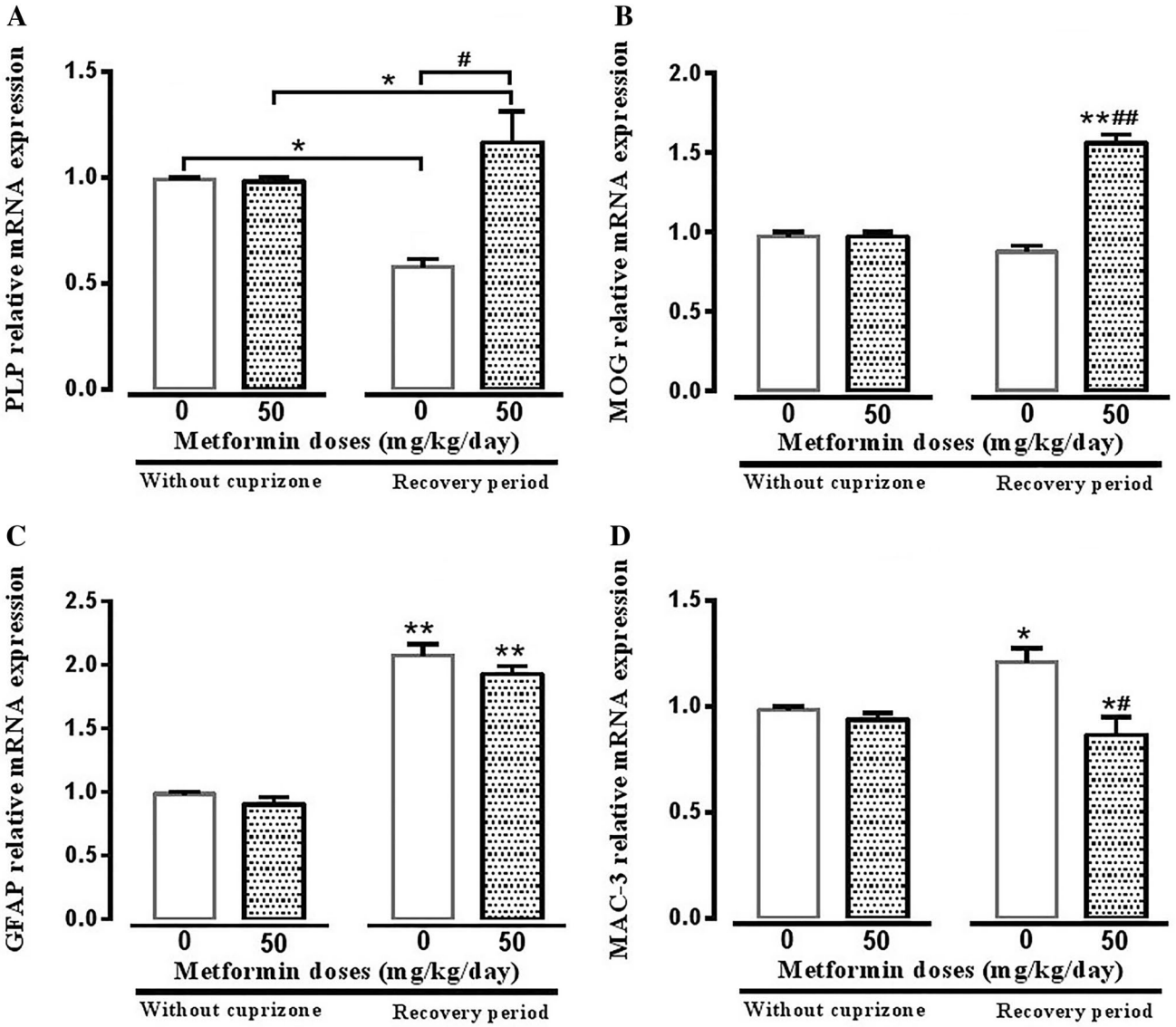

Fig. 3 Evaluation of effects of metformin (MET) in mRNA expression of myelin proteins (PLP and MOG) and glial markers (GFAP and Mac-3) by q-PCR method in corpus callosum (CC) (**a**–**d**). Quantification of results shows that recovery with MET significantly increased mRNA expression of PLP ($p < 0.05$), MOG ($p < 0.01$) and Mac-3 ($p < 0.05$) but did not any significant effect on GFAP mRNA expression in the comparison with free recovery period ($p < 0.05$, **a**, **b**). Data are presented as mean ± SEM, analyzed using tow-way ANOVA. *Compared to relevant control mice, #compared to free recovery, ($^{*,\#}p < 0.05$; $^{**,\#\#}p < 0.01$) with Bonferroni's correction for multiple comparisons

markers PLP ($p < 0.05$) and MOG ($p < 0.01$) when recovery was accompanied with MET compared to the free recovery group (Fig. 3a, b). As predicted, even after 1-week of the free recovery period, the levels of GFAP ($p < 0.01$) and Mac-3 ($p < 0.05$) mRNA were higher compared to the CPZ control group (Fig. 2a–c). Moreover, we observed a significant increase in Mac-3 ($p < 0.05$) but not in GFAP mRNA expression in the MET recovery group compared to the free recovery group (Fig. 3c, d).

Metformin downregulates apoptotic signaling cascades

For the investigation of the apoptosis-related signaling, WB analysis was performed for the flagship markers such as Bax/α-tubulin, Bcl-2/α-tubulin, cleaved caspase-3/α-tubulin and Bax/Bcl-2 ratios were measured in all experimental groups (Fig. 4a–d). WB results showed persistence of apoptotic signals even after the 1-week free recovery period compared to the CPZ control group ($p < 0.05$, Fig. 4b, d). Administration of MET during the 7 days of recovery period had a significant protective effect by increasing Bcl-2/α-tubulin ratio in comparison with the free recovery group (Fig. 4a). Notably, MET exerted its protective effect through intensive elevation of anti-apoptotic protein Bcl-2 level instead of decreasing apoptotic protein Bax level (Fig. 4b). Recovery with MET significantly decreased the Bax/Bcl-2 ratio ($p < 0.05$), in comparison with the free recovery group (Fig. 4c). Alternatively, administrating MET during recovery period reduced cleaved caspase-3/α-tubulin ratio indicating apoptosis reduction ($p < 0.05$, Fig. 4d).

Metformin increased recruitment of oligodendrocytes precursor cells

To study the intrinsic myelin regeneration capacity (recruitment of OPCs), flow cytometry, immunostaining and qRT-PCR assays for the O4 (late-stage) and NG-2 (early-stage) OPCs markers were performed in all experimental groups. Flow cytometry for O4 and NG-2 (in vivo analysis) indicated that both were expressed with different patterns in all experimental groups (Fig. 5a). In the free recovery group, there was a slight increase (from 2.19 to 4.51%) in the papulation of NG-2^+/$O4^+$ double-positive cells (represent OPCs in the transition-stage) in the CC compared to the CPZ control group (Fig. 5a). But in MET recovery group, NG-2^+/$O4^+$ populations was increased by 10.79% compared to the free recovery group (Fig. 5a). MET treatment dramatically

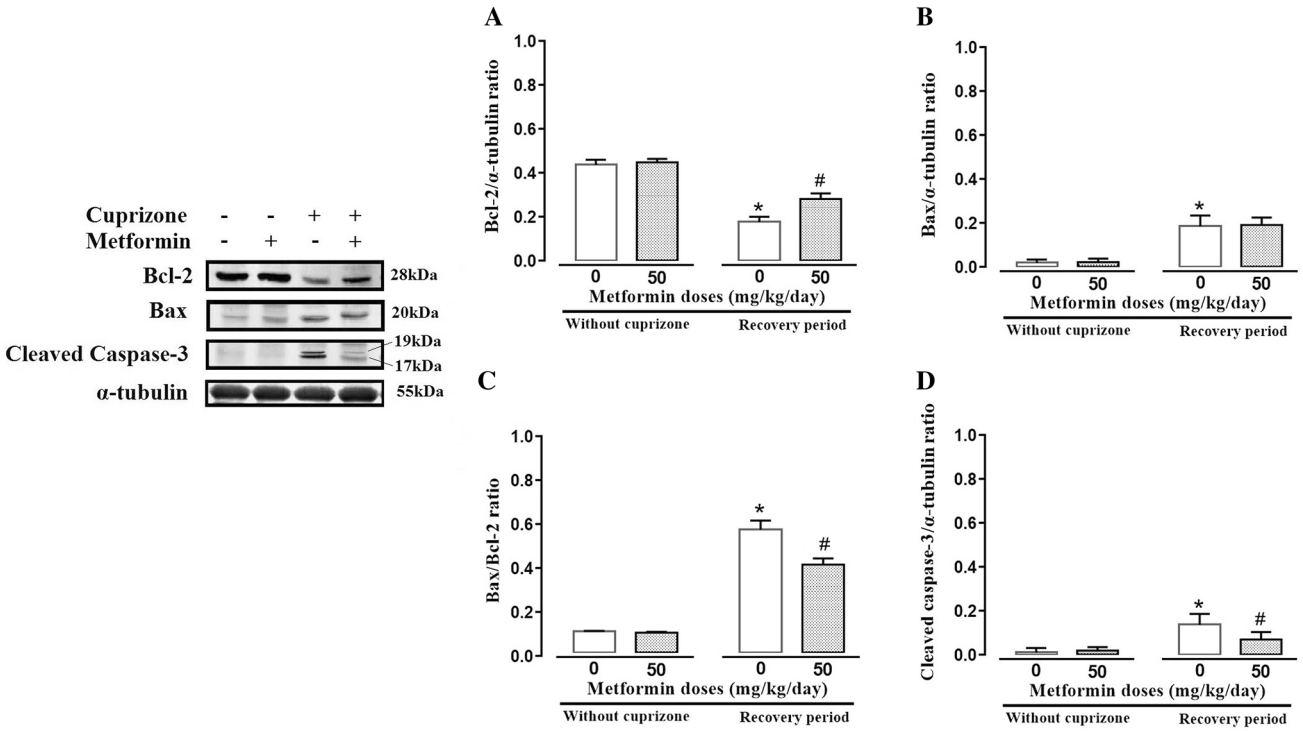

Fig. 4 Evaluation of effects of metformin (MET) in protein expression of apoptosis markers (Bax, Bcl-2, and cleaved Caspase-3) by WB method in corpus callosum (CC) (**a**–**d**). Quantification of results show that recovery with MET significantly decreased Bax/Bcl-2 ratio (**c**, $p < 0.05$), and cleaved caspase-3/α-tubulin ratio (**d**, $p < 0.05$) in the comparison with free recovery period. Data are presented as mean ± SEM, analyzed using tow-way ANOVA. *Compared to relevant control mice, #compared to free recovery, ($^{*,\#}p < 0.05$) with Bonferroni's correction for multiple comparisons

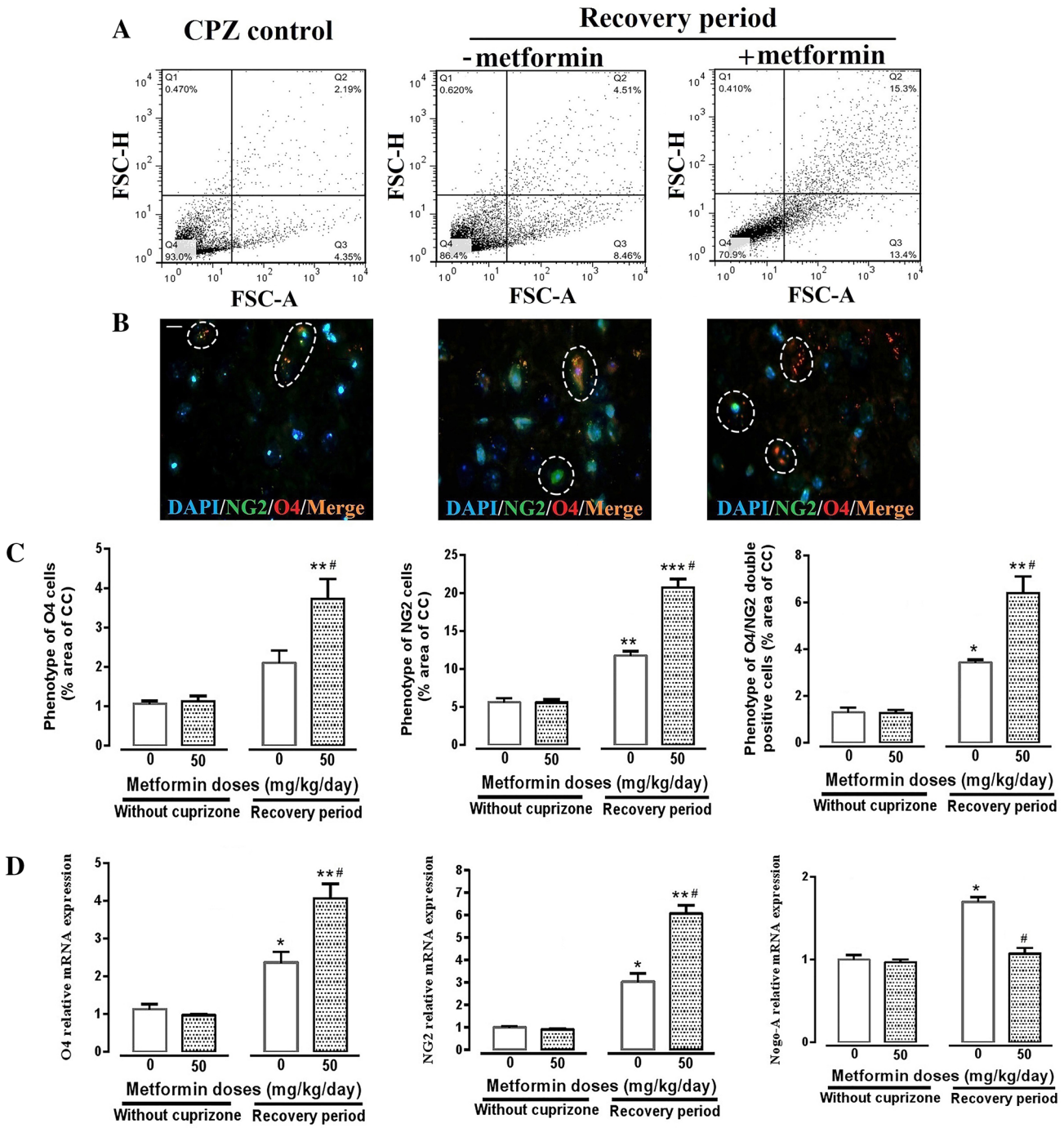

Fig. 5 Evaluation of effects of metformin (MET) in OLGs population (O4 and NG2) in corpus callosum (CC) (**a**–**d**). Flow cytometery with double staining of O4 and NG2 showed both markers were expressed in control and the recovery groups (**a**). In free recovery group, there was a minor increase (from 2.19 to 4.51%) in $O4^{+}/NG\text{-}2^{+}$ double-positive OPCs (transition-stage) in the CC compared to the control group (**a**). In MET recovery group, $O4^{+}/NG\text{-}2^{+}$ population increased by 10.79% compared to the free recovery group (**a**). One-week recovery with MET increased NG-2^{+} cells population by 4.94% in contrast to the free recovery group (**a**). Moreover, in MET recovery group O4 population only increased by 0.15% in contrast to the free recovery group (**a**). IHC of coronal sections through the CC for NG2 (green), O4 (red) and DAPI nuclear stain (blue) for in situ analysis of OPCs were performed (Fig. 4b, c). NG2 and O4 double-staining shows increased immunoreactivity after 1-week recovery period with MET in comparison with free recovery period (**b**, **c**). In addition, previous data have been confirmed by q-PCR analysis of NG2 and O4 mRNA expression in CC (3D). Expression of Nogo-A as negative controller of remyelination has been significantly decreased during MET recovery period in comparison with free recovery period (**d**). Scale bar = 50 µm. Data are presented as mean ± SEM, analyzed using tow-way ANOVA. *Compared to relevant control mice, $^{\#}$compared to free recovery, ($^{*,\#}p < 0.05$; $^{**}p < 0.01$; $^{***}p < 0.001$) with Bonferroni's correction for multiple comparisons

increased NG-2$^+$ population (NG-2$^+$/O4$^-$ represent a unique type of glial cell) by 4.94% in contrast to the free recovery group (Fig. 5a). Moreover, in MET recovery group, O4 population (NG-2$^-$/O4$^+$ represent a premature OLGs cell) was increased only by 0.15% in contrast to the free recovery group (Fig. 5a). IHC double staining for O4 and NG-2 (in situ analysis) confirmed previous findings and both markers were significantly overexpressed in the MET recovery group in contrast to the free recovery group (Fig. 5b, c). Indeed, MET treatment significantly increased the numbers of O4 ($p<0.05$) and NG-2 ($p<0.05$) positive cells in CC compared to the free recovery group (Fig. 5b, c). Furthermore, qRT-PCR also showed a significant increase in O4 ($p<0.05$) and NG-2 ($p<0.05$) mRNA expression and decrease in Nogo-A (negative controller of myelination) mRNA expression ($p<0.05$) in the MET recovery group compared to the free recovery group (Fig. 5d).

Metformin induced activation AMPK and inactivation of mTOR in oligodendrocytes

Double-staining of cells with mature oligodendrocyte marker (MOG) beside either mTOR or AMPK were carried out to localize active form of following markers (p-AMPK and p-mTOR) in CC region (Fig. 6a, b). Double-staining of cells with MOG and p-mTOR showed that population of MOG$^+$ cells was not altered by MET treatment but it significantly declined p-mTOR and these mice did not exhibit significant changes in MOG$^+$/p-mTOR$^+$ double-positive cells compared to control group (Fig. 6a). Recovery by MET significantly increased the numbers of MOG$^+$ cells ($p<0.05$) and decreased p-mTOR$^+$ cells ($p<0.05$) but slightly decreased MOG$^+$/p-mTOR$^+$ double-positive cells in CC compared to the free recovery group (Fig. 6a). On the other hand, double-stained MOG with p-AMPK indicated that MET considerably increased ($p<0.01$) p-AMPK, but had no substantial effect on the population of MOG$^+$/p-AMPK$^+$ double-positive cells compared to the control mice that were not treated by MET (Fig. 6b). However, MET recovery notably increased the numbers of both p-AMPK$^+$ cells ($p<0.05$) and MOG$^+$/p-AMPK$^+$ double-positive cells ($p<0.05$) in CC compared to the free recovery group (Fig. 6b).

Metformin induced activation of Nrf2 in oligodendrocytes

Double-staining of mature OLGs marker (MOG) besides p-Nrf2 was done to localize the active form of Nrf2

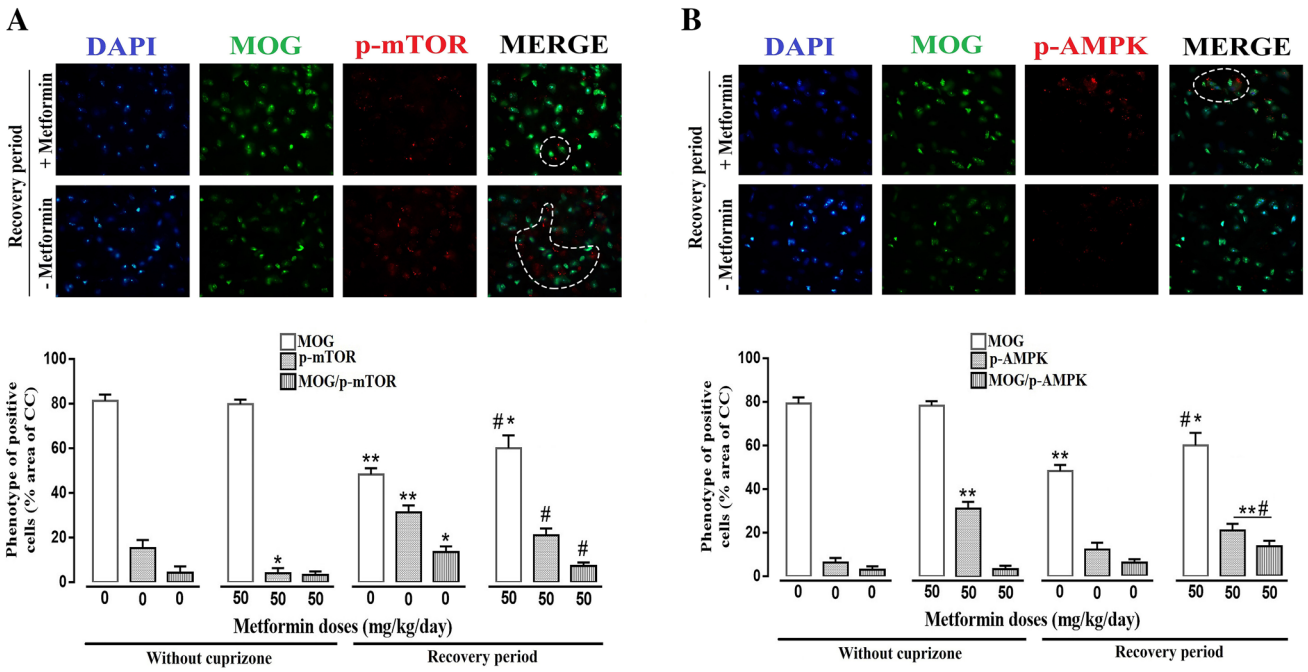

Fig. 6 Evaluation of effects of metformin (MET) in m-TOR and AMPK activation in mature OLGs (**a**, **b**). IHC of coronal sections through the CC showing labelling with a monoclonal antibody that is specific to MOG (green), p-AMPK (red) and p-mTOR (red), along with DAPI nuclear stain (blue) (**a**, **b**). p-mTOR staining shows significantly decreased in immunoreactivity after 1-week recovery period with MET in comparison with free recovery period ($p<0.05$, **a**). p-AMPK staining shows significantly increased in immunoreactivity after 1-week recovery period with MET in comparison with free recovery period ($p<0.05$, **b**). Scale bar = 50 µm. Data are presented as mean ± SEM, analyzed using tow-way ANOVA. *Compared to relevant control mice, $^{\#}$compared to free recovery, ($^{*,\#}p<0.05$; $^{**}p<0.01$) with Bonferroni's correction for multiple comparisons

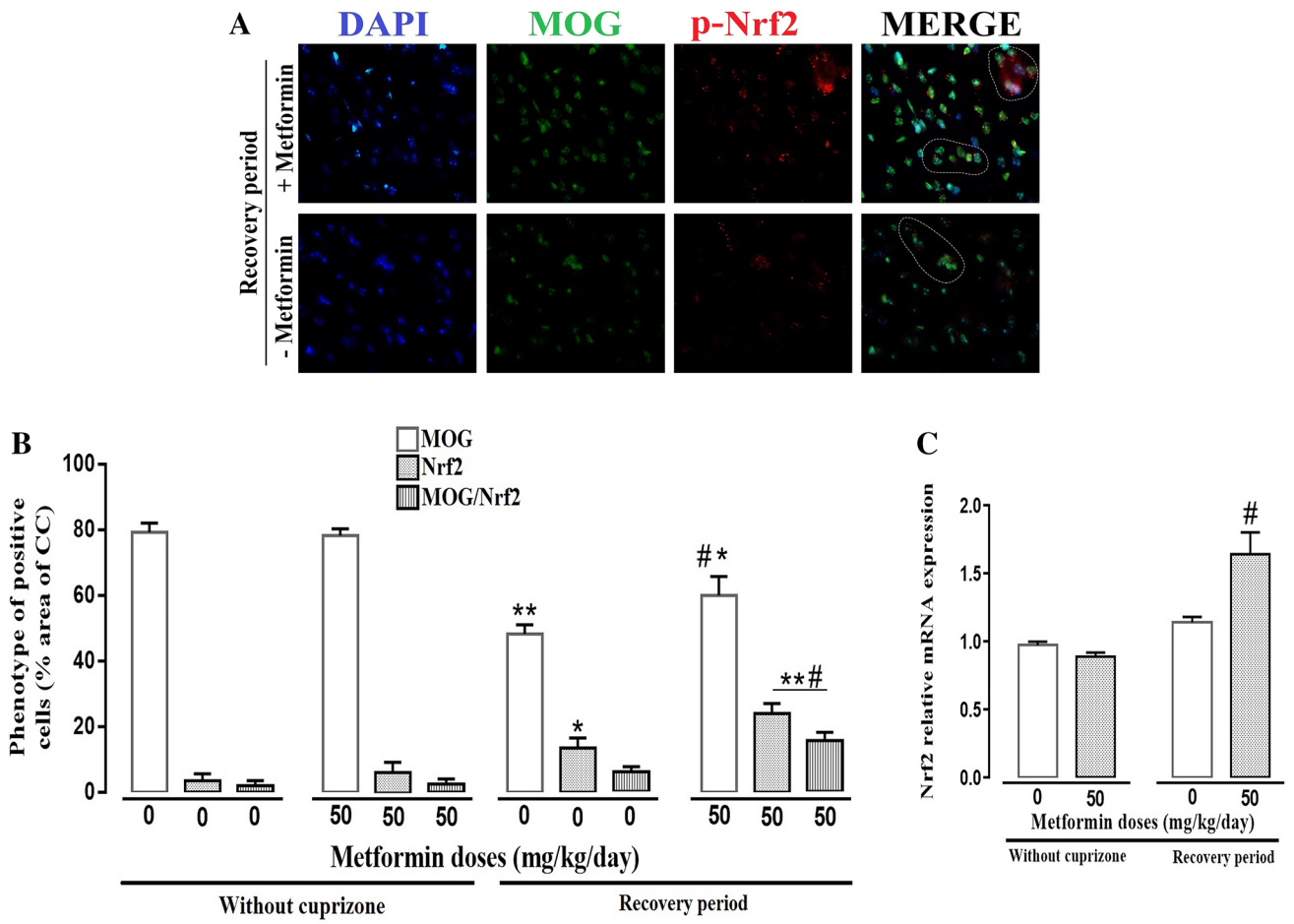

Fig. 7 Evaluation of effects of metformin (MET) in Nrf2 activation in mature OLGs (**a**–**c**). IHC of coronal sections through the CC showing labelling with a monoclonal antibody that is specific to MOG (green), p-Nrf2 (Red), along with DAPI nuclear stain (blue) (**a**). p-Nrf2 staining shows significantly increased in immunoreactivity after 1-week recovery period with MET in comparison with free recovery period ($p < 0.05$, **a**). In addition, this observation has been confirmed by q-PCR analysis of Nrf2 mRNA expression in CC (**c**). Expression of Nrf2 has been significantly increased during MET recovery period in comparison with free recovery period ($p < 0.05$, **b**). Scale bar = 50 µm. Data are presented as mean ± SEM, analyzed using tow-way ANOVA. *Compared to relevant control mice, $^{\#}$compared to free recovery, ($^{*,\#}p < 0.05$; $^{**}p < 0.01$) with Bonferroni's correction for multiple comparisons

(p-Nrf2) in CC region (Fig. 7a, b). IHC stained MOG and p-Nrf2 indicated that MET did not significantly affect either MOG^+, p-$Nrf2^+$ and MOG^+/p-$Nrf2^+$ double-positive cells in the control mice compared to the control mice that were not treated by MET (Fig. 7a, b). Double-staining of cells with an anti-MOG and anti-p-Nrf2 antibodies indicated that recovery with MET remarkably increased the numbers of MOG^+, p-$Nrf2^+$ and MOG^+/p-$Nrf2^+$ cells in CC compared to the free recovery group (Fig. 7a, b). Also by qRT-PCR analysis, we observed a significant increase in Nrf2 mRNA expression in MET recovery group compared to the free recovery group ($p < 0.05$, Fig. 7c).

Effects of metformin on redox signals and ADP/ATP ratio

Antioxidant index

Effects of MET on antioxidant indexes were measured in all experimental groups. Antioxidant indexes; namely CAT, SOD and GPx were significantly decreased after 5 weeks of CPZ treatment in comparison with mice fed with normal chow (data not shown). On the other hand, CAT ($p < 0.01$), SOD ($p < 0.01$) and GPx ($p < 0.05$) were significantly increased after 1-week free recovery period in comparison with mice fed with the normal chow

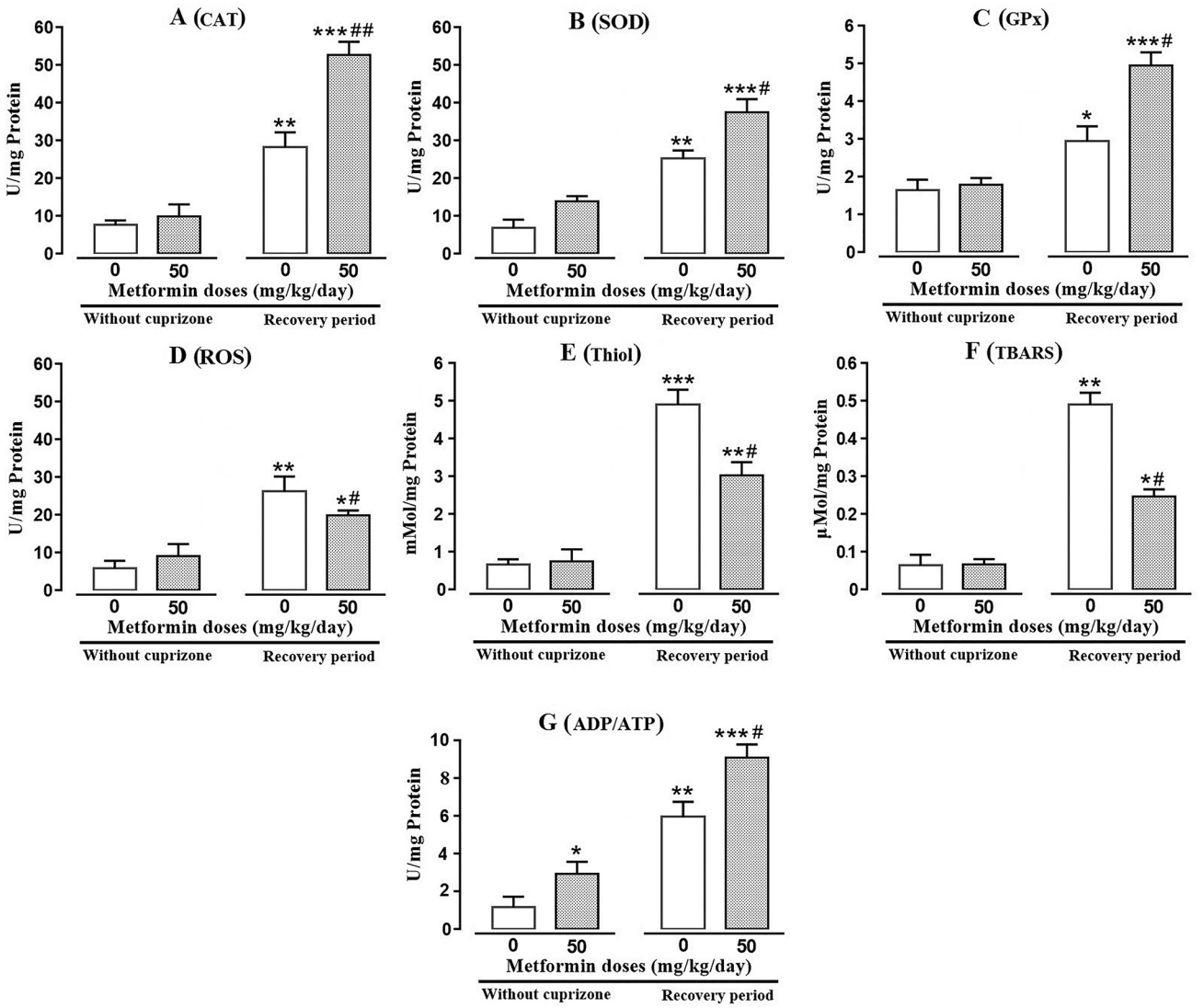

Fig. 8 Effects of metformin (MET) on oxidant and antioxidant indexes in coronal slices in corpus callosum (CC). Oxidant index; reactive oxygen spices (ROS), Thiol and TBARS were significantly decreased after recovery with MET in comparison with free recovery period ($p < 0.05$). Antioxidant index; catalase (CAT), superoxide dismutase (SOD) and glutathione (GPx) were significantly increased after recovery with MET in comparison with free recovery period ($p < 0.01$, $p < 0.05$ and $p < 0.05$ respectively). ADP/ATP level was significantly increased after recovery with MET in comparison with free recovery period ($p < 0.05$). Data are presented as mean ± SEM, analyzed using tow-way ANOVA. *Compared to relevant control mice, #compared to free recovery, ($^{*,\#}p < 0.05$; $^{**,\#\#}p < 0.01$; $^{***}p < 0.001$) with Bonferroni's correction for multiple comparisons

(Fig. 8a–c). Administration of MET during recovery period, had an undeniable protective effect by increasing CAT ($p < 0.01$), SOD ($p < 0.05$) and GPx ($p < 0.05$) indexes in comparison with the free recovery group (Fig. 8a–c). Metformin administration in control mice did not have a significant effect on the concentration of catalase, SOD, and glutathione in comparison with mice receiving vehicle (Fig. 8a–c).

Oxidant index

Effects of MET on oxidant indexes in coronal slices in CC were measured in all experimental groups. Oxidant indexes; namely ROS, Thiol and TBARS were significantly increased after 5 weeks of CPZ treatment in comparison with mice fed with the normal chow (data not shown). On the other hand, ROS ($p < 0.01$), Thiol ($p < 0.001$) and

TBARS ($p < 0.01$) were significantly increased after 1-week free recovery period in comparison with mice fed with the normal chow (Fig. 8d–f). Administration of MET during the 7 days of recovery period had a significant protective effect by decreasing ROS ($p < 0.05$), Thiol ($p < 0.05$) and TBARS ($p < 0.05$) indexes in comparison with the free recovery group (Fig. 8d–f). Metformin administration in the control mice did not have a significant effect on the concentration of ROS, Thiol and TBARS in comparison with mice receiving vehicle (Fig. 8d–f).

ADP/ATP ratio

Extracellular ADP/ATP ratio was remarkably decreased after 5 weeks of CPZ treatment in comparison with mice fed with the normal chow (data not shown). On the other hand, extracellular ADP/ATP ratio was remarkably increased ($p < 0.01$) after 1-week free recovery period in comparison with mice fed with the normal chow (Fig. 8g). Administration of MET during the 7 days of recovery period increased extracellular ADP/ATP ratio ($p < 0.05$) in comparison with the free recovery group (Fig. 8g). Remarkably, MET administration in control mice increased extracellular ADP/ATP ratio ($p < 0.05$) in comparison with mice receiving vehicle (Fig. 8g).

Molecular modeling

Molecular modeling techniques were used to understand the atomic details of the molecular mechanism of interaction between MET and AMPK in comparison with other proteins involved in the energy regulation pathway, including Nrf2-Keep1, MTORC1 and MTORC2. The obtained results are in agreement with experimental data and confirm the specific activity effects of MET on AMPK. On the one hand, the interaction of MET with other proteins shows a weak and unstable connection that can be indicative of the ineffectiveness, or the insignificant and inadequate effects of the MET on other pathways. On the other hand, the interaction site of MET on the AMPK molecule is entirely consistent with the location and mode of interaction of its main activator, AMP, which, in accordance with the experimental results, indicated its positive effects through the direct increase of AMPK activation (Fig. 9 and Table 2).

Table 2 Docking results of metformin interaction with target proteins

Molecule	ΔG bonding affinity (Kcal/mol)	Number in cluster
AMPK	−6.3	128
Keep1	−4.1	110
MTORC1	−3.8	135
MTORC2	−4.3	98

Discussion

In this manuscript, we have studied diabetes medication, metformin (MET), for myelin repair during post-demyelination recovery (regeneration/remyelination) period in the CPZ model of toxic demyelination after CPZ cessation.

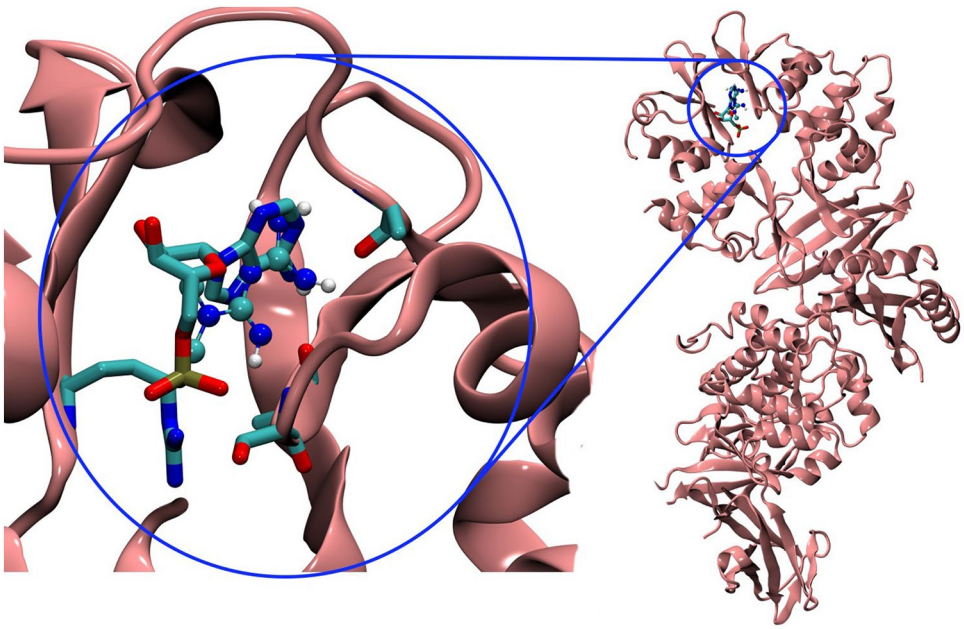

Fig. 9 Docking studies of metformin on AMPK. Crystal structure of AMPK-metformin docked complex

CPZ-induced myelin loss after 5 weeks and this acute demyelination could be endogenously repaired after an appropriate recovery period and CPZ cessation. Therefore, this model is similar to the sign of the pathophysiology of primary progressive MS and to a lesser extent progressive relapsing MS with the exception that in human subjects endogenous repair occurred gradually [33]. Moreover, CPZ induced the OLGs dystrophy equivalent to what happened in MS lesions (type III) [34].

AMPK/mTOR pathway is one of the important regulators of the cellular metabolism that is activated during stress conditions and depletion of ATP in the cell. AMPK inhibition leading to hindering of autophagy and attenuation of astrocytes viability in the case of oxygen and glucose deprivation [35]. Under the stress situations, AMPK inhibits processes that utilize energy and activates the catabolic pathways inside the cell. Moreover, mTOR is essential for controlling many pathways, such as cell growth, autophagy, insulin signaling, and transport of nutrients to cell [35]. On the other hand, due to the interaction between the metabolism and redox state, it is proposed that Nrf2 and AMPK may cooperate in exerting of MET protective effects.

We exhibited that MET-mediated AMPK activation could accelerate myelin recovery and improve behavioral dysfunctions. Here, we examined whether these effects are exerted through cross-talk between AMPK/Nrf2/mTOR axis or other signaling pathways are involved. Increasing of Nrf2 expression in OLGs confirmed that MET was involved in the control of the redox status in these cells through either AMPK activation or mTOR inactivation. In our study, administration of MET significantly improved motor impairment and decreased anxiety, which was manifested by an increase in oligodendrogenesis accompanied by decreased apoptosis signaling. The reduced behavioral dysfunctions and promoted neurogenesis might be due to the activation of protein kinase C-CREB binding protein (PKC-CBP) pathway [36]. Apparently, OLGs apoptosis is a vital feature in the pathogenesis of MS and caspase-mediated death of OLGs is critical for demyelination [37]. Our study showed that MET-induced AMPK activation is able to control brain apoptosis by decreasing cleaved caspase-3 and increasing Bcl_2 protein levels. Growing evidence suggests that AMPK/mTOR pathway may participate in neuroinflammation, neurodegeneration and protection of neurons from apoptosis through enhancing neuronal autophagy [38–41]. MET-induced mTOR inhibition could maintain the levels of ATP in OLGs, specifically when oxidative phosphorylation is impaired after redox imbalance [42, 43]. Several studies have shown that oxidative damage of OLGs and axonal dystrophy occurred in initial phases of active MS lesions and oxidative stress also impairs OPCs differentiation by epigenetic mechanisms such as histone acetylation [44–46]. In this regard, our study showed that MET prevents brain apoptosis and even promotes endogenous myelin repair via migration of OPCs to the lesion site.

It has been shown that AMPK signaling attenuated ROS generation by reduction of activity of NADPH oxidase, and MDA levels accompanied by overexpression of SOD [16, 47]. A detoxifying factor Nrf2 has an important role in the protection of the cells from oxidative stress via binding to the cis-acting element called the antioxidant responsive element (ARE) [48–50]. Nrf2 knockdown inhibits the cell proliferation and it also reduces the intracellular ATP level [51]. Our study confirms that AMPK activation is exquisitely coupled to mitochondrial metabolism through the increase of the cellular ADP/ATP ratio. This may be moderately due to identified effects of MET on the disruption of ROS, Thiol and TBARS production or induction of CAT, SOD, and GPx production.

It is also shown that antioxidant response proteins like Nrf2 are elevated in MS lesions and Nrf2 activation induced by AMPK is believed to have a key role in the pathogenesis of various diseases including pathogenic and neurodegenerative disorders [52, 53]. On the other hand, the reduction of Nrf2 caused activation of AMPK and inhibition of the mTOR pathway and loss of function mutation in Nrf2 resulted in the mTOR activation [52, 54]. Ashabi et al. [55] indicated that pretreatment by MET protects hippocampal neurons via increasing Nrf2 antioxidant pathway in cerebral ischemia. We propose that under CPZ-induced oxidative stress, MET enhances Nrf2-mediated antioxidant response in OLGs and activation of the related enzymes, thus, paving a way for a permissive environment for recruitment and maturation of OPCs.

An extensive population of OLGs lineage exists within the adult CNS, but do not express proteins such as myelin basic protein (MBP) and 2, 3-cyclic nucleotide 3-phosphodiesterase (CNP) as a mature OLGs markers. Instead, these cells have phenotypic characteristics of a more immature stage of the OLGs lineage. They express the platelet-derived growth factor α-receptor (PDGFRα), in addition to O4 and the NG2, all widely accepted as markers for OPCs throughout development. However, $NG2^+$ cells residing in the adult CNS do not resemble embryonic or neonatal $NG2^+$ cells in terms of their morphology or proliferation characteristics, but instead represent a unique type of glial cell that has the ability to react rapidly to CNS damage [56, 57].

Remarkably, MET treatment dramatically increased $NG\text{-}2^+/O4^-$ population of glial cell and decreased MAC-3 mRNA expression on the lesion site. This function could be resulting in the repopulation of the beneficial glial cell instead of harmful and inflammatory cells in an unidentified pathway.

It has been shown that A2B5/PDGFRα double-positive cells are the main population during early progenitor stage of OPCs differentiation. In the late progenitor stage, A2B5/

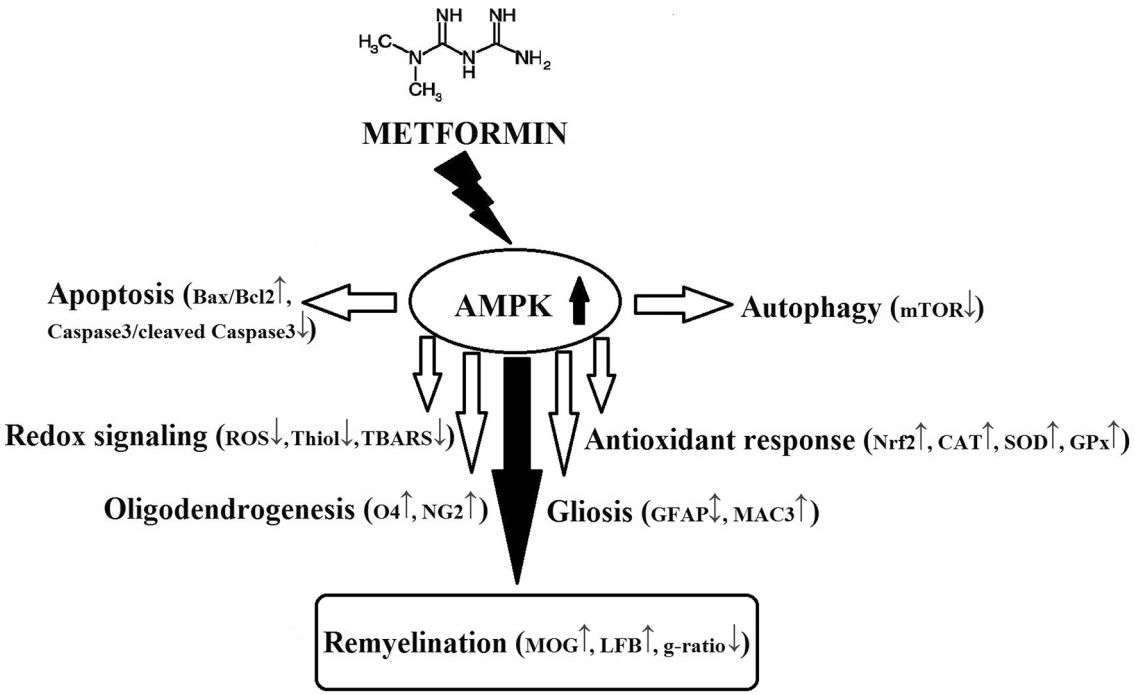

Fig. 10 Schematic description of the cell and molecular effects of metformin on myelin repair during recovery period after acute cuprizone-induced demyelination

PDGFRα was disappeared and O4 marker was observed. In the premyelinating OLGs, the expression of NG2 was increased, while the expression of O4 decreased compared to the previous stage. Finally, the myelinating OLGs expressed less NG2, which were highly positive for MOG, a major protein involved in the myelination process [32]. In accordance with these expression patterns, our study confirmed that MET significantly promoted the recruitment of intermediate ($NG2^+O4^+$) and premature ($NG2^-O4^+$) OPCs to lesion site probably through regulation of AMPK/Nrf2 pathway. Molecular modeling studies similarly confirmed the experimental results indicating that MET has an effective interaction with AMPK and ineffective interface with both Nrf2 and mTOR. It is predicted that the protective effect of MET on an abundance of OLGs and remyelination are not limited to CC and it is recapitulated in other CNS regions, as a consequence of CPZ challenge.

On the other hand, Nogo-A protein, a potent inhibitor of neurite growth, is the member of the reticulon proteins and exert several functions such as the regulation of growth and synaptic plasticity in the CNS [58]. It has been reported that silencing Nogo-A promotes functional recovery in demyelinating disease [59]. In this study, the recovery along with metformin significantly decreased the expression of Nogo-A mRNA. Our previous finding indicated that consumption of metformin during recovery period potentially induced p-AMPK and promoted repopulation of mature OLGs through up-regulation of neurotropic factors as well as recruitment of $Olig2^+$ precursor cells [60]. In accordance with our results, Largani and their colleagues recently showed that co-administration of CPZ and MET (oral gavage of 100 mg/kg) for 6 weeks improved mitochondrial hemostasis and increased myelinated axons via upregulating the expression of mitochondrial biogenesis genes and ameliorating the astrogliosis, microgliosis and oxidative stress induced by CPZ [61]. We should mention that this group only focused on the prophylactic effect (with co-administration with CPZ) of MET but not its therapeutic effects (administration after CPZ cessation).

Taken together, we observed that MET-induced AMPK activation triggers cell and molecular mechanisms that accelerate oligodendrogenesis and improves behavioral deficits during the 1-week recovery period (Fig. 10). This study showed the corporation of the energy sensitive signaling (AMPK/mTOR) and redox signaling (Nrf2) for the elevation of OLGs regeneration and myelin repair after acute demyelination.

Conclusion

Altogether, we conclude that MET induced myelin regeneration by increasing the number of OPCs ($NG2^+/O4^+$ cells) and regulation of mTOR/AMPK signaling pathway. Further,

MET also stimulates Nrf2-related antioxidant pathway, and therefore prevents apoptosis and moderates acute gliosis and ultimately provides a suitable condition for endogenous myelin renovation. Undoubtedly, further studies are necessary to determine whether pharmacological or genetic inhibition of AMPK phosphorylation prevents the MET neuroprotective effects, and to justify the reliance of p-AMPK as the key player in similar conditions. To date, this is the first study that provides a shared of objective evidence for the description of MET-enhanced remyelination via adjustment of AMPK/Nrf2/mTOR signaling in CNS.

Acknowledgements We are grateful to Dr. M. Baeiri from the Institute of Pharmaceutical Sciences (TIPS) at TUMS for her technical support.

Author contributions NS, FG, and FH, conceived and designed the study. All authors contributed to performing the relevant experiments. NS, MB, FG, and FH, analyzed the data. NS, and FG, wrote the paper. All authors contributed to reviewing and editing the manuscript and also read and approved the manuscript.

Funding This work was supported by the Iran University of Medical Sciences and University of Zabol (UOZ-GR-9618-5).

Compliance with ethical standards

Conflict of interest There is no potential conflict of interest or competing interest.

References

1. Sanadgol N, Zahedani SS, Sharifzadeh M, Khalseh R, Barbari GR, Abdollahi M. Recent updates in imperative natural compounds for healthy brain and nerve function: a systematic review of implications for multiple sclerosis. Curr Drug Targets. 2017;18(13):1499–517.
2. Belikov AV, Schraven B, Simeoni L. T cells and reactive oxygen species. J Biomed Sci. 2015;22:85.
3. Annibali V, Mechelli R, Romano S, Buscarinu MC, Fornasiero A, Umeton R, Ricigliano VA, Orzi F, Coccia EM, Salvetti M, Ristori G. IFN-β and multiple sclerosis: from etiology to therapy and back. Cytokine Growth Factor Rev. 2015;26(2):221–8.
4. Prantner D, Perkins DJ, Vogel SN. AMP-activated kinase (AMPK) promotes innate immunity and antiviral defense through modulation of stimulator of interferon genes (STING) signaling. J Biol Chem. 2017;292(1):292–304.
5. Meares GP, Qin H, Liu Y, Holdbrooks AT, Benveniste EN. AMP-activated protein kinase restricts IFN-gamma signaling. J Immunol. 2013;190(1):372–80.
6. Lyons C, Roche H. Nutritional modulation of AMPK-impact upon metabolic-inflammation. Int J Mol Sci. 2018;19(10):E3092.
7. Potter WB, O'Riordan KJ, Barnett D, Osting SM, Wagoner M, Burger C, Roopra A. Metabolic regulation of neuronal plasticity by the energy sensor AMPK. PLoS ONE. 2010;5(2):e8996.
8. Evans AM, Mahmoud AD, Moral-Sanz J, Hartmann S. The emerging role of AMPK in the regulation of breathing and oxygen supply. Biochem J. 2016;473(17):2561–72.
9. Zimmermann K, Baldinger J, Mayerhofer B, Atanasov AG, Dirsch VM, Heiss EH. Activated AMPK boosts the Nrf2/HO-1 signaling axis—a role for the unfolded protein response. Free Radic Biol Med. 2015;88(Pt B):417–26.
10. Ju TC, Chen HM, Chen YC, Chang CP, Chang C, Chern Y. AMPK-alpha1 functions downstream of oxidative stress to mediate neuronal atrophy in Huntington's disease. Biochim Biophys Acta. 2014;1842(9):1668–80.
11. Kim JE, Kim YW, Lee IK, Kim JY, Kang YJ, Park SY. AMP-activated protein kinase activation by 5-aminoimidazole-4-carboxamide-1-beta-D-ribofuranoside (AICAR) inhibits palmitate-induced endothelial cell apoptosis through reactive oxygen species suppression. J Pharmacol Sci. 2008;106(3):394–403.
12. Ceolotto G, Gallo A, Papparella I, Franco L, Murphy E, Iori E, Pagnin E, Fadini GP, Albiero M, Semplicini A, Avogaro A. Rosiglitazone reduces glucose-induced oxidative stress mediated by NAD(P)H oxidase via AMPK-dependent mechanism. Arterioscler Thromb Vasc Biol. 2007;27(12):2627–33.
13. Singh I, Samuvel DJ, Choi S, Saxena N, Singh AK, Won J. Combination therapy of lovastatin and AMP-activated protein kinase activator improves mitochondrial and peroxisomal functions and clinical disease in experimental autoimmune encephalomyelitis model. Immunology. 2018;154(3):434–51.
14. Nath N, Khan M, Rattan R, Mangalam A, Makkar RS, de Meester C, Bertrand L, Singh I, Chen Y, Viollet B, Giri S. Loss of AMPK exacerbates experimental autoimmune encephalomyelitis disease severity. Biochem Biophys Res Commun. 2009;386(1):16–20.
15. Blazquez C, Geelen MJ, Velasco G, Guzmán M. The AMP-activated protein kinase prevents ceramide synthesis de novo and apoptosis in astrocytes. FEBS Lett. 2001;489(2–3):149–53.
16. Paintlia AS, Paintlia MK, Mohan S, Singh AK, Singh I. AMP-activated protein kinase signaling protects oligodendrocytes that restore central nervous system functions in an experimental autoimmune encephalomyelitis model. Am J Pathol. 2013;183(2):526–41.
17. Sanadgol N, Golab F, Askari H, Moradi F, Ajdary M, Mehdizadeh M. Alpha-lipoic acid mitigates toxic-induced demyelination in the corpus callosum by lessening of oxidative stress and stimulation of polydendrocytes proliferation. Metab Brain Dis. 2018;33(1):27–37.
18. Sanadgol N, Golab F, Mostafaie A, Mehdizadeh M, Abdollahi M, Sharifzadeh M, Ravan H. Ellagic acid ameliorates cuprizone-induced acute CNS inflammation via restriction of microgliosis and down-regulation of CCL2 and CCL3 pro-inflammatory chemokines. Cell Mol Biol (Noisy-le-grand). 2016;62(12):24–30.
19. Jiang T, Yu JT, Zhu XC, Wang HF, Tan MS, Cao L, Zhang QQ, Gao L, Shi JQ, Zhang YD, Tan L. Acute metformin preconditioning confers neuroprotection against focal cerebral ischaemia by pre-activation of AMPK-dependent autophagy. Br J Pharmacol. 2014;171(13):3146–57.
20. Buzzai M, Jones RG, Amaravadi RK, Lum JJ, DeBerardinis RJ, Zhao F, Viollet B, Thompson CB. Systemic treatment with the antidiabetic drug metformin selectively impairs p53-deficient tumor cell growth. Cancer Res. 2007;67(14):6745–52.
21. Sanadgol N, Golab F, Mostafaie A, Mehdizadeh M, Khalseh R, Mahmoudi M, Abdollahi M, Vakilzadeh G, Taghizadeh G, Sharifzadeh M. Low, but not high, dose triptolide controls neuroinflammation and improves behavioral deficits in toxic model of multiple sclerosis by dampening of NF-κB activation and acceleration of intrinsic myelin repair. Toxicol Appl Pharmacol. 2018;342:86–98.
22. Vakilzadeh G, Khodagholi F, Ghadiri T, Darvishi M, Ghaemi A, Noorbakhsh F, Gorji A, Sharifzadeh M. Protective effect of a cAMP analogue on behavioral deficits and neuropathological changes in cuprizone model of demyelination. Mol Neurobiol. 2015;52(1):130–41.
23. Ramroodi N, Khani M, Ganjali Z, Javan MR, Sanadgol N, Khalseh R, Ravan H, Sanadgol E, Abdollahi M. Prophylactic

effect of BIO-1211 small-molecule antagonist of VLA-4 in the EAE mouse model of multiple sclerosis. Immunol Invest. 2015;44(7):694–712.
24. Sanadgol N, Golab F, Tashakkor Z, Taki N, Moradi Kouchi S, Mostafaie A, Mehdizadeh M, Abdollahi M, Taghizadeh G, Sharifzadeh M. Neuroprotective effects of ellagic acid on cuprizone-induced acute demyelination through limitation of microgliosis, adjustment of CXCL12/IL-17/IL-11 axis and restriction of mature oligodendrocytes apoptosis. Pharm Biol. 2017;55(1):1679–87.
25. Baeeri M, Momtaz S, Navaei-Nigjeh M, Niaz K, Rahimifard M, Ghasemi-Niri SF, Sanadgol N, Hodjat M, Sharifzadeh M, Abdollahi M. Molecular evidence on the protective effect of ellagic acid on phosalone-induced senescence in rat embryonic fibroblast cells. Food Chem Toxicol. 2017;100:8–23.
26. Askari H, Seifi B, Kadkhodaee M, Sanadgol N, Elshiekh M, Ranjbaran M, Ahghari P. Protective effects of hydrogen sulfide on chronic kidney disease by reducing oxidative stress, inflammation and apoptosis. EXCLI J. 2018;17:14–23.
27. Askari H, Abazari MF, Ghoraeian P, Torabinejad S, Nouri Aleagha M, Mirfallah Nassiri R, Tahmasebi F, Abedi N, Rajani SF, Salarian A, Belaran M, Elshiekh M, Sanadgol N. Ameliorative effects of hydrogen sulfide (NaHS) on chronic kidney disease-induced brain dysfunction in rats: implication on role of nitric oxide (NO) signaling. Metab Brain Dis. 2018;33(6):1945–54.
28. Aghajani M, Vaez Mahdavi MR, Najafabadi MK, Ghazanfari T, Moradi F, Golchoobian R, Askari H, Sanadgol N, Moghaddam EK. Depressed immune responses and accelerated splenic apoptosis due to experience of food deprivation and inequality but not unstable social status in Balb/c mice. NeuroImmunoModulation. 2017;24(4–5):200–10.
29. Shirazi MK, Azarnezhad A, Abazari MF, Poorebrahim M, Ghoraeian P, Sanadgol N, Bokharaie H, Heydari S, Abbasi A, Kabiri S, Aleagha MN, Enderami SE, Dashtaki AS, Askari H. The role of nitric oxide signaling in renoprotective effects of hydrogen sulfide against chronic kidney disease in rats: involvement of oxidative stress, autophagy and apoptosis. J Cell Physiol. 2019;234(7):11411–23.
30. Hosseini A, Sharifzadeh M, Rezayat SM, Hassanzadeh G, Hassani S, Baeeri M, Shetab-Bushehri V, Kuznetsov DA, Abdollahi M. Benefit of magnesium-25 carrying porphyrin-fullerene nanoparticles in experimental diabetic neuropathy. Int J Nanomed. 2010;5:517–23.
31. Poorebrahim M, Asghari M, Abazari MF, Askari H, Sadeghi S, Taheri-Kafrani A, Nasr-Esfahani MH, Ghoraeian P, Aleagha MN, Arab SS, Kennedy D, Montaseri A, Mehranfar M, Sanadgol N. immunomodulatory effects of a rationally designed peptide mimetic of human Ifnβ in Eae model of multiple sclerosis. Prog Neuropsychopharmacol Biol Psychiatry. 2018;82:49–61.
32. Robinson AP, Rodgers JM, Goings GE, Miller SD. Characterization of oligodendroglial populations in mouse demyelinating disease using flow cytometry: clues for MS pathogenesis. PLoS ONE. 2014;9(9):e107649.
33. Jennings AR, Carroll WM. Oligodendrocyte lineage cells in chronic demyelination of multiple sclerosis optic nerve. Brain Pathol. 2015;25(5):517–30.
34. Praet J, Guglielmetti C, Berneman Z, Van der Linden A, Ponsaerts P. Cellular and molecular neuropathology of the cuprizone mouse model: clinical relevance for multiple sclerosis. Neurosci Biobehav Rev. 2014;47:485–505.
35. Agarwal S, Agarwal S, Tiwari SK, Seth B, Yadav A, Singh A, Mudawal A, Chauhan LK, Gupta SK, Choubey V, Tripathi A, Kumar A, Ray RS, Shukla S, Parmar D, Chaturvedi RK. Activation of autophagic flux against xenoestrogen bisphenol-A-induced hippocampal neurodegeneration via AMP kinase (AMPK)/mammalian target of rapamycin (mTOR) pathways. J Biol Chem. 2015;290(34):21163–84.
36. Wang J, Gallagher D, DeVito LM, Cancino GI, Tsui D, He L, Keller GM, Frankland PW, Kaplan DR, Miller FD. Metformin activates an atypical PKC-CBP pathway to promote neurogenesis and enhance spatial memory formation. Cell Stem Cell. 2012;11(1):23–35.
37. Caprariello AV, Mangla S, Miller RH, Selkirk SM. Apoptosis of oligodendrocytes in the central nervous system results in rapid focal demyelination. Ann Neurol. 2012;72(3):395–405.
38. Gong X, Gong X, Wang H, Ye Y, Shu Y, Deng Y, He X, Lu G, Zhang S. miR-124 regulates cell apoptosis and autophagy in dopaminergic neurons and protects them by regulating AMPK/mTOR pathway in Parkinson's disease. Am J Transl Res. 2016;8(5):2127–37.
39. Peixoto CA, Oliveira WH, Araújo SMDR, Nunes AKS. AMPK activation: role in the signaling pathways of neuroinflammation and neurodegeneration. Exp Neurol. 2017;298(Pt A):31–41.
40. Xue H, Xue H, Ji Y, Wei S, Yu Y, Yan X, Liu S, Zhang M, Yao F, Lan X, Chen L. HGSD attenuates neuronal apoptosis through enhancing neuronal autophagy in the brain of diabetic mice: the role of AMP-activated protein kinase. Life Sci. 2016;153:23–34.
41. Culmsee C, Monnig J, Kemp BE, Mattson MP. AMP-activated protein kinase is highly expressed in neurons in the developing rat brain and promotes neuronal survival following glucose deprivation. J Mol Neurosci. 2001;17(1):45–58.
42. Zhou Z, Chen S, Zhao H, Wang C, Gao K, Guo Y, Shen Z, Wang Y, Wang H, Mei X. Probucol inhibits neural cell apoptosis via inhibition of mTOR signaling pathway after spinal cord injury. Neuroscience. 2016;329:193–200.
43. Zheng X, Boyer L, Jin M, Kim Y, Fan W, Bardy C, Berggren T, Evans RM, Gage FH, Hunter T. Alleviation of neuronal energy deficiency by mTOR inhibition as a treatment for mitochondria-related neurodegeneration. eLife. 2016;5:e13378.
44. Haider L, Fischer MT, Frischer JM, Bauer J, Höftberger R, Botond G, Esterbauer H, Binder CJ, Witztum JL, Lassmann H. Oxidative damage in multiple sclerosis lesions. Brain. 2011;134(Pt 7):1914–24.
45. Fischer MT, Sharma R, Lim JL, Haider L, Frischer JM, Drexhage J, Mahad D, Bradl M, van Horssen J, Lassmann H. NADPH oxidase expression in active multiple sclerosis lesions in relation to oxidative tissue damage and mitochondrial injury. Brain. 2012;135(Pt 3):886–99.
46. French HM, French HM, Reid M, Mamontov P, Simmons RA, Grinspan JB. Oxidative stress disrupts oligodendrocyte maturation. J Neurosci Res. 2009;87(14):3076–87.
47. Wang S, Zhang M, Liang B, Xu J, Xie Z, Liu C, Viollet B, Yan D, Zou MH. AMPKalpha2 deletion causes aberrant expression and activation of NAD(P)H oxidase and consequent endothelial dysfunction in vivo: role of 26S proteasomes. Circ Res. 2010;106(6):1117–28.
48. Niu NK, Wang ZL, Pan ST, Ding HQ, Au GH, He ZX, Zhou ZW, Xiao G, Yang YX, Zhang X, Yang T, Chen XW, Qiu JX, Zhou SF. Pro-apoptotic and pro-autophagic effects of the Aurora kinase A inhibitor alisertib (MLN8237) on human osteosarcoma U-2 OS and MG-63 cells through the activation of mitochondria-mediated pathway and inhibition of p38 MAPK/PI3K/Akt/mTOR signaling pathway. Drug Des Dev Ther. 2015;9:1555–84.
49. Zhang H, Liu YY, Jiang Q, Li KR, Zhao YX, Cao C, Yao J. Salvianolic acid A protects RPE cells against oxidative stress through activation of Nrf2/HO-1 signaling. Free Radic Biol Med. 2014;69:219–28.
50. Huang H, Taraboletti A, Shriver LP. Dimethyl fumarate modulates antioxidant and lipid metabolism in oligodendrocytes. Redox Biol. 2015;5:169–75.
51. Jia Y, Jia Y, Wang H, Wang Q, Ding H, Wu H, Pan H. Silencing Nrf2 impairs glioma cell proliferation via AMPK-activated mTOR inhibition. Biochem Biophys Res Commun. 2016;469(3):665–71.

52. van Horssen J, Drexhage JA, Flor T, Gerritsen W, van der Valk P, de Vries HE. Nrf2 and DJ1 are consistently upregulated in inflammatory multiple sclerosis lesions. Free Radic Biol Med. 2010;49(8):1283–9.
53. Mo C, Wang L, Zhang J, Numazawa S, Tang H, Tang X, Han X, Li J, Yang M, Wang Z, Wei D, Xiao H. The crosstalk between Nrf2 and AMPK signal pathways is important for the anti-inflammatory effect of berberine in LPS-stimulated macrophages and endotoxin-shocked mice. Antioxid Redox Signal. 2014;20(4):574–88.
54. Shibata T, Saito S, Kokubu A, Suzuki T, Yamamoto M, Hirohashi S. Global downstream pathway analysis reveals a dependence of oncogenic NF-E2-related factor 2 mutation on the mTOR growth signaling pathway. Cancer Res. 2010;70(22):9095–105.
55. Ashabi G, Khalaj L, Khodagholi F, Goudarzvand M, Sarkaki A. Pre-treatment with metformin activates Nrf2 antioxidant pathways and inhibits inflammatory responses through induction of AMPK after transient global cerebral ischemia. Metab Brain Dis. 2015;30(3):747–54.
56. Polito A, Reynolds R. NG2-expressing cells as oligodendrocyte progenitors in the normal and demyelinated adultcentral nervous system. J Anat. 2005;207(6):707–16.
57. El Waly B, Macchi M, Cayre M, Durbec P. Oligodendrogenesis in the normal and pathological central nervous system. Front Neurosci. 2014;8:145.
58. Kempf A, Schwab ME. Nogo-A represses anatomical and synaptic plasticity in the central nervous system. Physiology. 2013;28(3):151–63.
59. Yang Y, Liu Y, Wei P, Peng H, Winger R, Hussain RZ, Ben LH, Cravens PD, Gocke AR, Puttaparthi K, Racke MK, McTigue DM, Lovett-Racke AE. Silencing Nogo-A promotes functional recovery in demyelinating disease. Ann Neurol. 2010;67(4):498–507.
60. Houshmand F, Sanadgol N, Barati M, Golab F, Ramezani-sefidar S, Tanbakooie S, Tabatabaei M, Amiri M. Metformin-induced AMPK activation stimulates remyelination through induction of neurotrophic factors, downregulation of NogoA and recruitment of Olig2 + precursor cells in the cuprizone murine model of multiple sclerosis. DARU J Pharm Sci. 2019. https://doi.org/10.1007/s40199-019-00286-z.
61. Largani SHH, Borhani-Haghighi M, Pasbakhsh P, Mahabadi VP, Nekoonam S, Shiri E, Kashani IR, Zendehdel A. Oligoprotective effect of metformin through the AMPK-dependent on restoration of mitochondrial hemostasis in the cuprizone-induced multiple sclerosis model. J Mol Histol. 2019;50(3):263–71.